J Med Primatol doi:10.1111/j.1600-0684.2008.00288.x

ORIGINAL ARTICLE

A rhesus monkey reference label atlas for template driven segmentation

Jonathan J. Wisco[1], Douglas L. Rosene[1,4], Ronald J. Killiany[1], Mark B. Moss[1,4], Simon K. Warfield[2,3], Svetlana Egorova[2], Ying Wu[2], Zsusanna Liptak[2], Jeremy Warner[1] & Charles R.G. Guttmann[2]

1 Laboratory for Cognitive Neurobiology, Department of Anatomy and Neurobiology, Boston University School of Medicine, Boston, MA, USA
2 Center for Neurological Imaging, Department of Radiology, Brigham and Women's Hospital, Harvard Medical School, Boston, MA, USA
3 Computational Radiology Laboratory, Department of Radiology, Brigham and Women's Hospital, Harvard Medical School, Boston, MA, USA
4 Yerkes National Primate Research Center, Emory University, Atlanta, GA, USA

Keywords
MRI – segmentation

Correspondence
Jonathan J. Wisco, PhD, Division of Integrative Anatomy, Department of Pathology and Laboratory Medicine, David Geffen School of Medicine at UCLA, 10833 Le Conte Ave., Room 52-060 CHS, Los Angeles, CA 90095-1732, USA.
Tel.: 310-825-7880;
fax: 310-825-3058;
e-mail: jjwisco@mednet.ucla.edu

Accepted November 15, 2007.

Abstract

Background We have acquired dual-echo spin-echo (DE SE) MRI data of the rhesus monkey brain since 1994 as part of an ongoing study of normal aging. To analyze these legacy data for regional volume changes, we have created a reference label atlas for the Template Driven Segmentation (TDS) algorithm.
Methods The atlas was manually created from DE SE legacy MRI data of one behaviorally normal, young, male rhesus monkey and consisted of 14 regions of interest (ROI's). We analyzed the reproducibility and validity of the TDS algorithm using the atlas relative to manual segmentation.
Results ROI volumes were comparable between the two segmentation methodologies, except TDS overestimated the volume of basal ganglia regions. Both methodologies were highly reproducible, but TDS had lower sensitivity and comparable specificity.
Conclusions TDS segmentation calculates accurate volumes for most ROI's. Sensitivity will be improved in future studies through the acquisition of higher quality data.

Introduction

The overall goal of this project was to develop an automated segmentation pipeline for the analysis of rhesus monkey MRI data that have been acquired since 1994 as part of an ongoing investigation of animal models for normal aging. Monkey subjects received regular MRI scans over their lifetime, making it desirable and necessary to use the same MRI protocol over the years. Here we present the creation and validation of a reference template atlas of the rhesus monkey brain for the automated segmentation technique, Template Driven Segmentation (TDS) [1].

Template Driven Segmentation requires a reference template atlas to provide *a priori* anatomical probability for the segmentation of statistically classified gray matter, white matter and cerebrospinal fluid (CSF) voxels into more specific regions of interest (ROI's). This segmentation tool has been used with a human reference atlas [1], but a rhesus monkey reference atlas for TDS has not been created. Styner and colleagues [2] have created a rhesus monkey reference atlas for a segmentation method similar in principle to TDS, but it was unusable for the study presented here because their atlas was created from data acquired with substantially different imaging parameters. Thus,

the first goal of the present study was to create such an atlas, which included forebrain white matter, cerebral cortex, caudate nucleus, putamen, globus pallidus, claustrum, thalamus, hypothalamus, brainstem, cerebellum, lateral ventricles, third ventricle, cerebral aqueduct and fourth ventricle ROI's. The atlas was created from the DE SE legacy image data set of one behaviorally normal, young adult (age 7) rhesus monkey. The second goal of the present study was to test the reproducibility and validity of TDS using the atlas compared to manual segmentation of the same ROI's.

Previously, TDS has been used successfully to segment brain images in studies of aging, multiple sclerosis (MS) and schizophrenia [1, 3–5]. TDS has proven to be an effective, efficient and reliable method to segment brains from large-scale studies with minimal operator interaction. This present work extends the application of TDS to a rhesus monkey animal model and compares the results of the automated method to manual segmentation by five operators.

Materials and methods

Animal subjects

Five male rhesus monkeys (5–10 years old) (AM053, AM099, AM056, AM093, AM052) were selected for this study from the colonies of the Yerkes National Primate Research Center (YNPRC). They were part of an ongoing study of normal aging that excluded subjects with splenectomy or thymectomy history, exposure to radiation, cancer, organ transplantation, malnutrition, chronic illness (including viral or parasitic infections), neurological disease, or chronic drug administration. Medical examinations were administered prior to entering the study, which included serum chemistry, hematology, urine analysis and fecal analysis. Quarterly tuberculosis tests, direct or indirect measurement of blood pressure, an electrocardiogram, and blood work (CBC, electrolytes, lipid profile) examinations were also administered to ensure continued health.

All monkeys in the present study were housed and cared for in the laboratory Animal Science Center at Boston University Medical Center (BUMC) where they were housed individually in colony rooms within auditory and visual range of other monkeys. They were all maintained on a normal diet consisting of Standard Purina Monkey Chow and under a 12-hour light/dark cycle with of a gradual transition of one hour between cycles. Feeding occurred once a day following behavioral testing, and water was available continually. The monkeys were also inspected daily by both animal care personnel and research technicians. All procedures were approved by the Institutional Animal Care and Use Committees (IACUC) of both YNPRC and BUMC. Both YNPRC and BUMC are fully accredited by the Association for the Assessment and Accreditation of Laboratory Animal Care (AAALAC) and all procedures conformed to the NIH Public Health Service Policy on Humane Care and Use of Laboratory Animals.

Imaging protocol

Monkeys were anaesthetized using a mixture of ketamine and xylazine for transport from the colony room to the MR scanner. Upon arrival, monkeys were placed in a 1.5T Signa GE scanner bore in the prone position. Their heads were stabilized in standard stereotactic space using 30 mm raised eye and ear bars in a non-ferrous stereotactic frame [6]. The ear bars marked the zero coordinate of the coronal plane. A 5-inch surface coil was then secured directly over the cranium, parallel to the horizontal axis of the stereotactic frame and just above the earbars. Anaesthesia level was monitored and maintained with supplementary doses for the duration of the image acquisition.

A localizer Fast Spin-echo (FSE) scan [TR = 2000 ms; TE = 90 ms; 5.0 mm slice; FOV = 256 × 192 mm; 1 nex] was acquired in the sagittal plane to assist with the orientation of the subsequent scan protocol.

The interleaved dual-echo spin-echo (DE SE) sequences [TR = 3000 ms; TE = 30/80 ms; 2.7 mm slice; FOV = 150 × 150 mm (256 × 256); 1 nex] yielded proton density- (pdw) and T2-weighted (T2w) images, acquired in the coronal plane. The series consisted of approximately 60 images (30 pdw, 30 T2w) covering the entire rostral to caudal extent of the forebrain and hindbrain. Anisotropic diffusion filtering was applied to the DE SE images to improve signal to noise ratio while preserving structure edges [7].

Creation of the reference atlas

The reference label atlas of the monkey brain was constructed by manual outlining of DE SE images of AM093 using 3D Slicer (http://www.slicer.org) after anisotropic diffusion filtering. Nissl stained histological sections from this monkey, digitized using the Inquiry digitizing system (Loats Associates, Inc.), and a published histological atlas [8] served as anatomical references for correctly labeling each ROI and for distinguishing low contrast brain structures. The pdw images provided good contrast between gray matter and white matter structures, whereas the T2w images

J Med Primatol (2008) 1–11

provided good contrast between brain structures and CSF surrounding the brain and within the ventricles.

The resulting atlas consisted of 14 manually segmented regions of interest (ROI's): forebrain white matter, cerebral cortex, caudate nucleus, putamen, globus pallidus, claustrum, thalamus, hypothalamus, brainstem, cerebellum, lateral ventricles, third ventricle, cerebral aqueduct and fourth ventricle. In addition, an intracranial cavity (ICC) label was created for providing the reference matrix for the first of two registration processes required for non-linear registration in the TDS algorithm. The operational definitions (below) begin with a description of reference landmarks followed by the atlas structures.

The DE SE data acquired since 1994 were obtained using the best available slice parameters at the time. Due to the anisotropic voxel dimensions, data were best viewed in the coronal plane. Cerebral cortex, forebrain white matter and lateral ventricle were easily distinguishable in this orientation. However, operationally defined landmarks assisted with the parcellation of the thalamus, hypothalamus, brainstem, cerebellum, third ventricle, cerebral aqueduct and fourth ventricle. These same definitions were provided to the individual raters as a guide for manual segmentations.

Operationally defined landmarks

The following landmarks were overlaid on the images of the atlas subject to guide the creation of the ROI's (Fig. 1).

Caudate-Putamen landmark: A line parallel to the internal capsule, separating the caudate medially from the putamen laterally where they are connected anteriorly by the nucleus accumbens. The nucleus accumbens is therefore distributed evenly (approximately) between the caudate and putamen.

Third ventricle landmark: An axial line just inferior to the body of the fornix.

Thalamus-Hypothalamus landmark: A line that extended from the vertical midpoint of the third ventricle to the most dorsal aspect of the hippocampus. This line was placed on slices where both the thalamus and hypothalamus were adjacent to each other.

Thalamus-Brainstem landmark: A line that extended from the most inferior point of the third ventricle to the most dorsal aspect of the hippocampus. This landmark was never present on the same image slice as the thalamus-hypothalamus landmark.

Lateral ventricle landmark: A line tangential to the lateral corner of the lateral geniculate nucleus of the thalamus. This landmark defined the medial border of the inferior horn of the lateral ventricles where the choroidal fissure was difficult to identify.

Brainstem-Cerebellum landmark: A parasagittal line along the lateral edge of the brainstem. Bilaterally, these two parallel lines would differentiate the brainstem from the cerebellum on image slices rostral to the appearance of the fourth ventricle such that brainstem is labeled between the lines, and the cerebellum is labeled outside the lines.

Fourth ventricle landmark: A line extended from the lateral corner of the fourth ventricle to the angle between the cerebellum folia and the brainstem. The landmark appeared on the first image slice where the fourth ventricle can be seen between the brainstem and cerebellum.

Operationally defined structures and regions

The following operational definitions for ROI's guided the creation of the atlas after operationally defined landmarks were overlaid on the images.

Intracranial Cavity (ICC): Included all pixels of the brain parenchyma and cerebrospinal fluid except the olfactory tract and the optic nerve rostral to the optic chiasm, and the brainstem inferior to the cerebellomedullary cistern.

Total forebrain: Included forebrain white matter, forebrain gray matter and ventricles.

Forebrain parenchyma: Included forebrain white matter and forebrain gray matter.

Forebrain white matter: Included all white matter of the cerebral hemispheres but not white matter contained within the deep gray matter structures of the basal ganglia, brainstem or cerebellum.

Forebrain gray matter: Included the cerebral cortex, caudate nucleus, putamen, globus pallidus, claustrum, thalamus and hypothalamus, but not the brainstem and cerebellum.

Cerebral cortex: Included cerebral cortex, basal forebrain, hippocampus and amygdala, but not nuclei of the deep gray matter.

Caudate Nucleus: Striatal gray matter medial to the Caudate-Putamen landmark, (including the medial portion of nucleus accumbens) extending throughout the body and tail.

Putamen: Striatal gray matter lateral to the Caudate-Putamen landmark (including the lateral portion of nucleus accumbens).

Globus Pallidus: Lenticular nucleus gray matter including internal and external segments, but not including the putamen.

Claustrum: Deep gray matter between putamen and insula surrounding external capsule and extending partially into the temporal stem white matter.

Thalamus: First visible posterior to the optic chiasm, one slice caudal to the first slice on which the

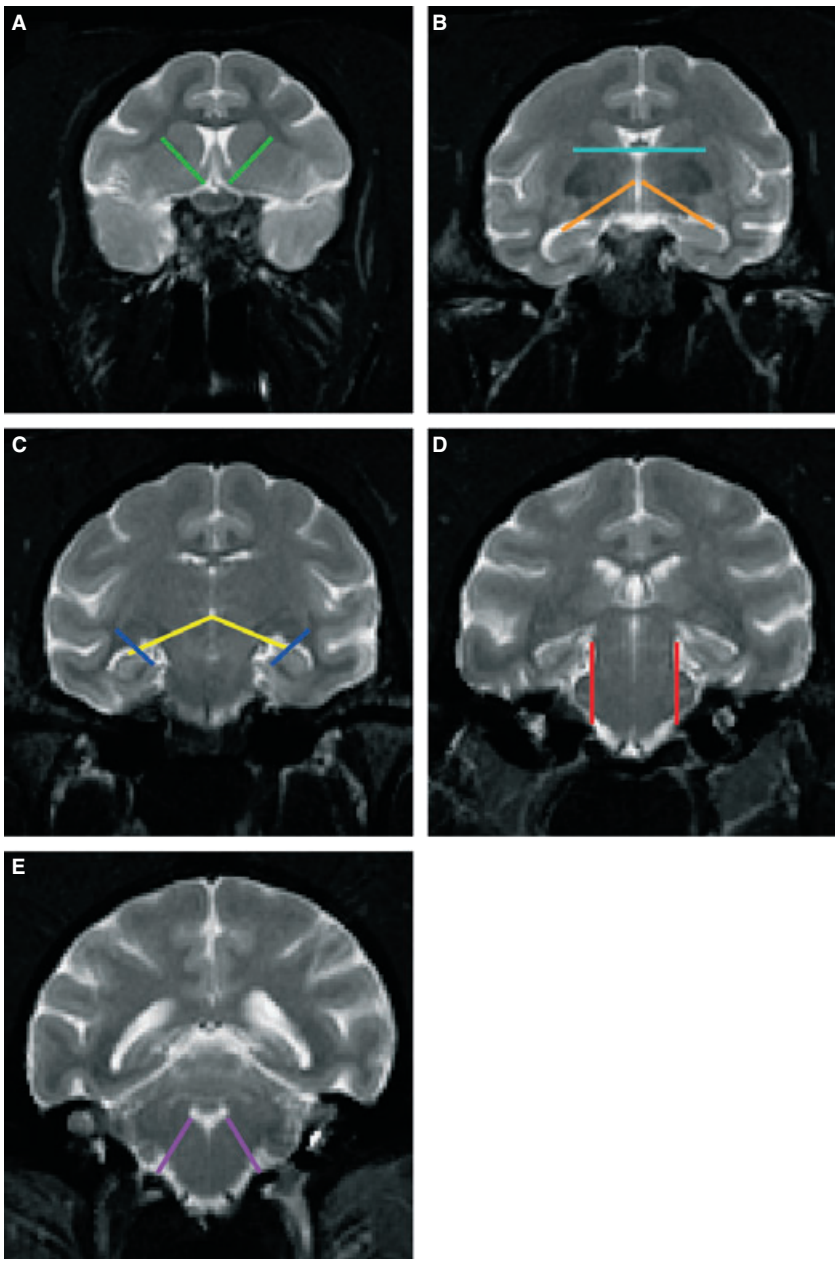

Fig. 1 Reference landmarks used to operationally define borders of regions of interest (ROI's). The image slices shown here are representative T2-weighted images of several slices in which the landmark was used by manual raters. Landmarks: caudate-putamen (A, green), third ventricle (B, light blue), thalamus-hypothalamus (B, orange), thalamus-brainstem (C, yellow), lateral ventricle (C, blue), brainstem-cerebellum (D, red), fourth ventricle (E, purple).

hypothalamus first appeared. The thalamus was distinguished from the hypothalamus by the thalamus-hypothalamus landmark. Caudal to the hypothalamus, the thalamus was distinguished from the brainstem by the thalamus-brainstem landmark.

Hypothalamus: First visible on the slice which exhibited the anterior commissure traversing across the midline. On this image the HYP was inferior to the anterior commissure. The thalamus and hypothalamus were distinguished by the thalamus-hypothalamus landmark.

Brainstem: Included all intrinsic white matter and gray matter demarcated by the thalamus-brainstem, brainstem-cerebellum and fourth ventricle landmarks. The brainstem was excluded on images caudal to the section where the cerebellomedullary cistern and fourth ventricle appear continuously.

J Med Primatol (2008) 1–11

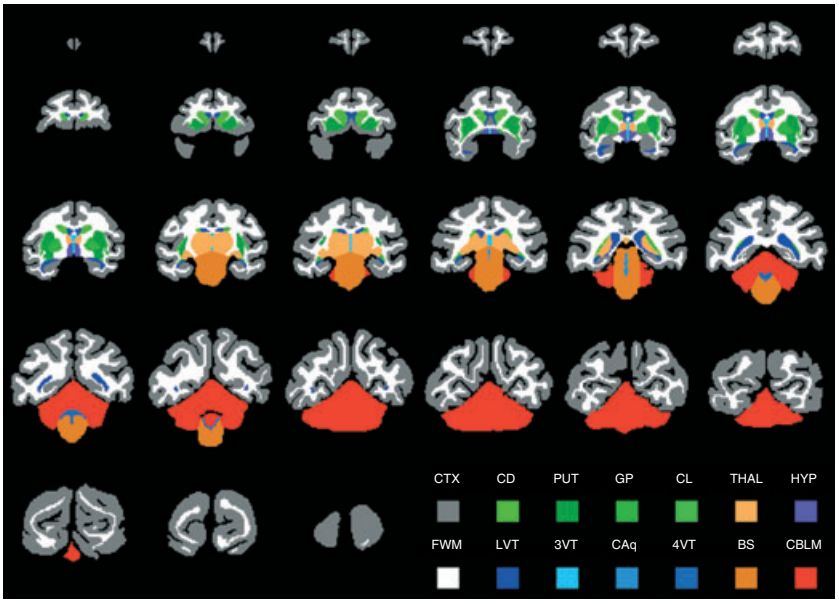

Fig. 2 Template atlas. Rostral to caudal slices in the coronal plane is arranged from top to bottom, left to right. Legend abbreviations: cortical gray matter (CTX), caudate nucleus (CD), putamen (PUT), globus pallidus (GP), claustrum (CL), thalamus (THAL), hypothalamus (HYP), forebrain white matter (FWM), lateral ventricles (LVT), 3rd ventricle (3VT), cerebral aqueduct (CAq), 4th ventricle (4VT), brainstem (BS), cerebellum (CBLM).

Cerebellum: Included all intrinsic white matter and gray matter structures demarcated by the brainstem-cerebellum and fourth ventricle landmarks and its interface with subarachnoid CSF and cerebral cortex. The fourth ventricle was not included.

Ventricular CSF: Sum of ventricular volumes.

Lateral ventricles: Included all CSF-associated pixels within the anterior horns, confluence, posterior horns and inferior horns. The lateral ventricle landmark was the medial border for the inferior horns.

Third ventricle: Included all CSF-associated pixels within the diencephalon, extending rostrally between the hemi-structures of the hypothalamus and caudally between the hemispheres of the posterior thalamus up to the transverse fissure. The superior border of the third ventricle was the third ventricle landmark.

Cerebral aqueduct: Included all CSF-associated pixels leading from the third ventricle to the fourth ventricle at the midline of the brainstem.

Fourth ventricle: Included the CSF-associated pixels just caudal to the cerebral aqueduct, between the cerebellum and brainstem as demarcated by the fourth ventricle line, not including the cerebellomedullary cistern.

Manual and automated image analysis protocols

Manual segmentation

Anisotropic diffusion filtering was applied to the DE SE images to improve signal to noise ratio [7]. Five raters (J.J.W., S.E., Y.W., Z.L., J.W.), working independently, manually segmented five DE SE legacy data sets using 3D Slicer. These raters ranged in research backgrounds including the pre-clinical sciences, anatomy, pharmacology and radiology. However, each rater was trained by the lead author of this paper (JJW) to recognize the borders of the 14 ROI's (forebrain white matter, cerebral cortex, caudate nucleus, putamen, globus pallidus, claustrum, thalamus, hypothalamus, brainstem, cerebellum, lateral ventricles, third ventricle, cerebral aqueduct and fourth ventricle) using the aforementioned operational landmarks and definitions. These were the same ROI's contained in the reference label atlas (Fig. 2). One rater repeated the manual segmentation for subjects AM093 and AM056.

Automated segmentation

The same data sets that were manually segmented were also automatically segmented using the TDS algorithm [1]. First, an intracranial cavity (ICC) was segmented from the interleaved DE SE images using a threshold function in 3D Slicer. Misclassifications of the intensity thresholding were manually corrected throughout the entire data set of each animal by a supervised rater. This was the only manual intervention in the automated pipeline. Second, pixels within the ICC were masked, and segmented using the 3D Expectation-Maximization (EM) [9, 10] for gray matter, white matter and cerebrospinal fluid (CSF) classes [11] without

user intervention. Finally, the gray matter- and white matter-classified pixels within the ICC became the input for TDS segmentation.

Template Driven Segmentation applied two steps of image registration: first, linear transformation between the reference atlas ICC and the observed ICC of the target case; second, non-rigid elastic matching (warping) of the reference atlas to the observed 3D EM segmentation input. Linear transformation (with three translation and three rotation parameters) was computed to align the ICC of the reference atlas to the ICC of each of the five animal subjects. Then, elastic matching was performed [12] to match surface and deep structural anatomy of the reference atlas to the 3D EM segmented images of each subject. The resulting atlas to subject match provided segmentation of the gray matter, white matter and CSF into the more specific 14 ROI's. The procedure was repeated for subjects AM093 and AM056.

Statistical analysis

For each subject, ROI volumes were normalized by dividing the ROI volume by the ICC volume. These normalized volumes were used for all statistical analyses such that 'ROI volume' always refers to a standardized measure.

Relative to manual segmentation, the quality of TDS segmentation was assessed by measuring its accuracy of volume calculation, its reproducibility and its validity. For any given ROI volume, we defined an acceptable TDS segmentation as being within two standard deviations of the manual segmentations mean (tested using the one-sample student's t-test). For the repeated manual and TDS segmentations of AM093 and AM056, we defined 95 percent reproducibility as acceptable. Validity was assessed by comparing the sensitivity and specificity of manual and TDS segmentations relative to a 'hidden ground truth' segmentation of each ROI volume. The ground truth was calculated using the Simultaneous Truth and Performance Level Estimation (STAPLE) algorithm described by Warfield and colleagues [13, 14]. In summary, the hidden ground truth segmentation for each ROI volume was calculated by STAPLE based on the manual segmentations of the subjects by the five raters. Then, each rater's sensitivity and specificity for each ROI volume was calculated relative to the ground truth. Finally, the mean sensitivity and specificity for manual segmentation was compared with that of TDS segmentation. Sensitivity was the proportion of ground truth segmentation correctly identified and specificity was the proportion of the non-ground truth segmentation correctly unidentified.

Results

Template Driven Segmentation was comparable (within the two standard deviation range) to manual segmentation for 11 of the 14 ROI's. For caudate, putamen and globus pallidus ROI's, TDS segmented volumes were outside the acceptable range of calculated volume (Table 1).

Both manual and TDS segmentation were highly reproducible. The repeated segmentation of two monkey brains resulted in over 95 percent reproducibility (i.e. 5 percent error) for the manual method and near 99 percent for TDS. The effective difference between the two methods was only evident in the amount of time taken to complete the segmentation of the entire brain. Whereas manual segmentation required at least three days to complete one brain, TDS segmentation completed one brain in three hours.

The Simultaneous Truth and Performance Level Estimation (STAPLE) algorithm was performed to determine the quality of TDS segmentation relative to the five raters. We found lower sensitivity values for all TDS segmented ROI volumes relative to the manually segmented volumes, but the specificity values were comparable (Table 1). Specificity values were comparable between the two methodologies.

Discussion

Summary of findings

This study produced several notable results. First, a 3D reference label atlas of the rhesus monkey brain was created and applied successfully with the TDS automated segmentation algorithm. Second, this study found that both manual and automated segmentation were highly reproducible, but automated segmentation required less than a tenth of the time to produce its results. Third, TDS agrees with segmentations performed by five, independent manual raters for all ROI's except caudate, putamen and globus pallidus.

Rationale for single-subject atlas

The application of the TDS algorithm to the segmentation of the rhesus monkey brain necessitated the creation of the reference label atlas, which served as the template for elastic matching to all other subject brains. As we were interested in anatomical changes of the brain, we were faced with the decision of whether to create a single-subject atlas or to create a composite atlas from a sample of brains. The argument in favor of either type of atlas has been debated among leading

J Med Primatol (2008) 1–11

Table 1 Manual segmentation vs. TDS segmentation. We considered a two standard deviation range for the manual raters as an acceptable target for TDS calculations. One-way student's t-test scores for TDS segmented ROI volumes that were significant (bold) ($P < 0.01$) indicate that the volume was beyond the operationally defined acceptable range. Sensitivity and specificity calculations were performed using the Simultaneous Truth and Performance Level Estimation (STAPLE) algorithm

	Manual segmentation				TDS segmentation			
ROI	Mean volume (cc)	2 SD range (cc)	Sensitivity mean (SD)	Specificity mean (SD)	Mean volume (cc)	t-test score	Sensitivity	Specificity
FWM	23.23	18.17–28.29	0.8063 (0.0388)	0.9992 (0.0003)	27.41	2.34	0.5854	0.9936
CTX	41.2	32.17–50.23	0.9857 (0.0033)	0.9996 (0.0002)	40.84	−0.11	0.8856	0.9985
CD	1.3	0.82–1.77	0.7988 (0.0323)	0.9985 (0.0005)	2.39	**6.5**	0.5345	0.9946
PUT	1.57	0.89–2.26	0.7754 (0.0362)	0.9984 (0.0005)	2.87	**5.33**	0.4619	0.9941
GP	0.56	0.32–0.79	0.7647 (0.0402)	0.9984 (0.0005)	1.25	**8.44**	0.4205	0.9942
CL	0.39	0–0.83	0.7651 (0.0403)	0.9984 (0.0005)	0.54	1	0.4235	0.9941
THAL	2.17	1.19–3.15	0.7908 (0.0330)	0.9984 (0.0005)	2.33	0.45	0.4986	0.9944
HYP	0.33	0.09–0.57	0.7612 (0.0399)	0.9984 (0.0005)	0.15	−2.19	0.4048	0.9943
BS	4.04	3.04–5.03	0.7617 (0.0417)	0.9993 (0.0002)	3.42	−1.74	0.5108	0.9954
CBLM	9.03	7.30–10.76	0.8314 (0.0290)	0.9985 (0.0005)	9.76	1.21	0.6026	0.9943
LVT	1.22	0.63–1.80	0.8107 (0.0368)	0.9992 (0.0003)	1.73	2.5	0.6005	0.9934
3VT	0.14	0.07–0.22	0.8106 (0.0368)	0.9992 (0.0003)	0.08	−2.37	0.6008	0.9934
CAq	0.04	0–0.07	0.8116 (0.0361)	0.9992 (0.0003)	0.06	1.54	0.6044	0.9934
4VT	0.14	0.01–0.27	0.8108 (0.0360)	0.9992 (0.0003)	0.17	0.64	0.6027	0.9934

FWM, forebrain white matter; CTX, cerebral cortex; CD, caudate nucleus; PUT, putamen; GP, globus pallidus; CL, claustrum; THAL, thalamus; HYP, hypothalamus; BS, brainstem; CBLM, cerebellum; LVT, lateral ventricles; 3VT, third ventricle; CAq, cerebral aqueduct; 4VT, fourth ventricle.

brain mapping researchers [15, 16], but both approaches have been accepted within the brain warping community.

Classic single-subject atlases [17–20] provide a reference to which all other subjects can be compared. The only concern for single-subject atlases is whether they can, in their implementation, provide adequate accuracy despite the failure to account for anatomical variability in the population. Composite atlases [12, 15, 16, 21–27] provide a working, dynamic reference based on statistical accuracy, and can improve over time as more data are acquired. These types of atlases are particularly useful for functional imaging studies, and characterize normal anatomy as a function of individual variability.

Compared to the human brain, the rhesus monkey brain does not exhibit a great deal of anatomical variability. Secular effects, such as changes in total brain volume over many generations, have not been observed in the rhesus monkey [28]. For these reasons, the single-subject atlas is well suited for the study of rhesus monkey brain anatomy.

Rationale for operational definitions

This work was motivated by an existing database of several hundred images of rhesus monkey brains acquired since 1994 for studies of normal aging. The imaging protocol was determined by the technology available at the time. Today, similar studies would be facilitated by the availability of scanners with higher magnetic field strengths and imaging protocols capable of higher resolution and isotropic voxel dimensions [2, 29]. Isotropic data is easily reconstructed into axial, coronal and sagittal orientations, yielding multiple views to aid manual raters in the segmentation of structures or regions. Unfortunately, the data collected since 1994 did not reconstruct well in the axial or sagittal orientation due to the anisotropic voxel dimensions. As a consequence, the operational definitions outlined for this particular dataset were a necessary guide for manual segmentation of the coronal slices, the only reliable orientation for viewing. Regardless of this limitation, the results for most structures from both manual and automated segmentation proved reasonable for statistical comparison. Due to the increasing overall quality of MR images, future studies will unlikely require the assistance of operational definitions in order to help raters distinguish structures.

Volume comparison

This study showed that the TDS segmented volumes of forebrain white matter, cerebral cortex, claustrum, thalamus, hypothalamus, brainstem, cerebellum, lateral ventricles, third ventricle, cerebral aqueduct and fourth ventricle ROI's were comparable within two

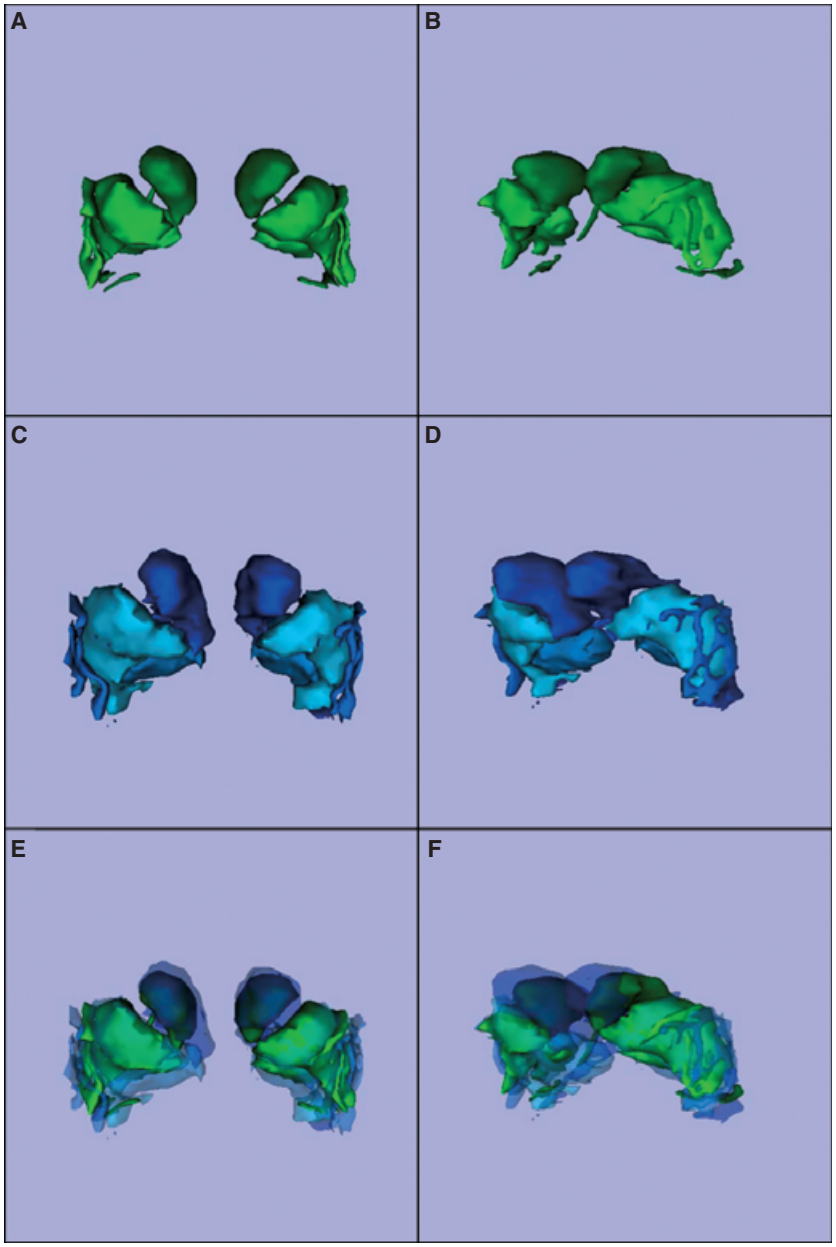

Fig. 3 Comparison of basal ganglia structures between manual segmentation and TDS segmentation. For simplicity of visualization, the 3D reconstruction of the manually segmented structures originates from only one of the five raters. Anterior view of manual segmentation (green) of basal ganglia structures (A); anterolateral view of manually segmented basal ganglia structures (B); anterior view of TDS segmentation (blue) of basal ganglia structures (C); anterolateral view of TDS segmented basal ganglia structures (D); anterior view of TDS segmentation superimposed over the manual segmentation of basal ganglia structures (E); anterolateral view of TDS segmentation superimposed over the manually segmented basal ganglia structures (F). Distinguishable color shades indicate separate structures. The basal ganglia structures included here are caudate nucleus (CD), putamen (PUT), globus pallidus (GP) and claustrum (CL).

standard deviations of manually segmented volumes. However, TDS overestimated the volumes for caudate, putamen and globus pallidus ROI's (Table 1, Fig. 3). These deep gray matter ROI's reside almost entirely within the forebrain white matter ROI. We hypothesize that caudate, putamen and globus pallidus ROI's were more sensitive to forebrain white matter warping. In contrast, the thalamus ROI is nearly surrounded by forebrain white matter, but the inferior portion borders the brainstem ROI. Even

J Med Primatol (2008) 1–11

though thalamus volume was slightly overestimated, perhaps its neighboring association with the brainstem minimized excessive non-linear deformation. TDS also underestimated the volumes of hypothalamus, brainstem and third ventricle by as much as 50 percent, although this was not significant. We also attribute this trend to the warping of surrounding white matter.

Reproducibility

Our results demonstrated that repeated segmentation of the 14 structures of interest contained in the reference label atlas could be accomplished with equally high reproducibility by a manual rater and by TDS. Given that each rhesus monkey brain requires approximately 3–4 days to segment using the manual tracing method, but at most several hours to segment using the automated pipeline, we conclude that TDS has a distinct cost-benefit advantage over manual segmentation. Thus, both precision and time required were vastly improved.

Validity

Volume measurements between the two segmentation methodologies were comparable, but TDS sensitivity was lower, ranging from 0.4048 to 0.8856 (Table 1). We found no association between ROI volume and sensitivity using a Spearman rank test (rho = 0.1209, $P = 0.6806$). Our interpretation of these results is that TDS accurately calculates volume, but only precisely calculates the spatial location of the ROI's.

Comparison of methodologies

The methodological approach of the two techniques differed in two major respects. First, manual segmentation was based on the visual contrast of structures seen in pdw and T2w images of the DE SE dataset, but TDS segmentation was based on the 3D EM statistical classification of gray matter, white matter and CSF. Thus, the decision process for classifying voxels affected by partial volume effects was based on human judgment or statistical calculation, respectively. Given the inhomogeneity of image quality in this legacy data set, the potential error in either methodology could have had an impact in the classification of voxels of ROI's within and between subjects.

Second, after raters classified voxels into gray matter, white matter and CSF, they used the operationally defined boundaries to further delineate these classes into more specific ROI's. In contrast, after 3D EM classified voxels into gray matter, white matter and CSF, TDS performed the non-linear deformation of the template atlas (with the operationally defined borders as an integral part of the ROI's) to the 3D EM segmented data. The difference between distinguishing operationally defined regions with a *post hoc* (manual segmentation) or *a priori* (TDS segmentation) strategy could contribute to the difference in sensitivity.

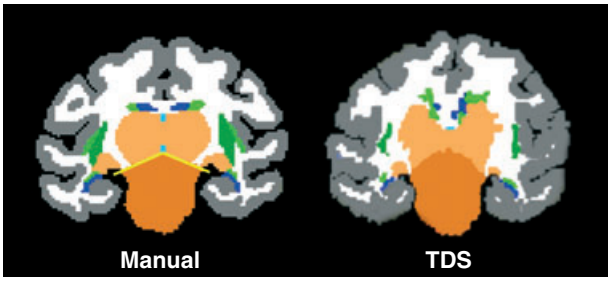

Fig. 4 Comparison of manual segmentation (left) with TDS segmentation (right). The thalamus-brainstem landmark from Fig. 1 has been overlaid in yellow. For ROI labels, please refer to color legend in Fig. 2.

To illustrate, Fig. 4 compares manual and TDS segmentation of a coronal slice just caudal to the globus pallidus. In the manually segmented image, the thalamus-brainstem operationally defined landmark from Fig. 1 has been overlaid in yellow to illustrate how a rater would distinguish the thalamus from the brainstem. In the TDS segmented image, this border was warped as part of the boundary between thalamus and brainstem. This phenomenon occurred for all the operationally defined landmarks and would account for the decreased sensitivity of TDS segmentation and the overestimation and underestimation of some smaller ROI volumes.

Future directions

This is our first step towards optimizing an automated segmentation algorithm for rhesus monkey MRI data. Here we compared two different methodological approaches to the segmentation of legacy data and found TDS to be faster and comparable in volume calculation. Sensitivity will be improved as we compare the segmentation of higher quality data that improves the signal to noise ratio and minimizes partial volume effects. In fact, we have already constructed a new head holder that allows for the positioning of the monkey cranium in the center of a multi-channel head coil as opposed to the surface head coil that was used in the acquisition of the data analyzed here.

Acknowledgments

This research was funded in part by the following funding agencies: National Institutes of Health (F31-AG 05897, P01-AG00001, P41-RR13218-01, P51-RR 000165, R01-NS35142, R37-AG176090), Whitaker Foundation, and Boston University School of Medicine Graduate Student Research Fellowship.

References

1 Warfield S, Dengler J, Zaers J, Guttmann CR, Wells WM 3rd, Ettinger GJ, Hiller J, Kikinis R: Automatic identification of gray matter structures from MRI to improve the segmentation of white matter lesions. *J Image Guid Surg* 1995; **1**:326–38.

2 Styner M, Knickmeyer R, Joshi S, Coe C, Short SJ, Gilmore J: Automatic brain segmentation in rhesus monkeys. *SPIE* 2007; **6512**:65122L.

3 Guttmann CR, Kikinis R, Anderson MC, Jakab M, Warfield SK, Killiany RJ, Weiner HL, Jolesz FA: Quantitative follow-up of patients with multiple sclerosis using MRI: reproducibility. *J Magn Reson Imaging* 1999; **9**:509–18.

4 Iosifescu DV, Shenton ME, Warfield SK, Kikinis R, Dengler J, Jolesz FA, McCarley RW: An automated registration algorithm for measuring MRI subcortical brain structures. *Neuroimage* 1997; **6**:13–25.

5 Wei X, Warfield SK, Zou KH, Wu Y, Li X, Guimond A, Mugler JP 3rd, Benson RR, Wolfson L, Weiner HL, Guttmann CR: Quantitative analysis of MRI signal abnormalities of brain white matter with high reproducibility and accuracy. *J Magn Reson Imaging* 2002; **15**:203–9.

6 Saunders RC, Aigner TG, Frank JA: Magnetic resonance imaging of the rhesus monkey brain: use for stereotactic neurosurgery. *Exp Brain Res* 1990; **81**:443–6.

7 Gerig G, Kubler O, Kikinis R, Jolesz FA: Nonlinear anisotropic filtering of MRI data. *IEEE Transactions on Medical Imaging* 1992; **11**:221–32.

8 Paxinos G, Huang X-F, Toga A: The Rhesus Monkey Brain in Stereotaxic Coordinates. San Diego, CA: Academic Press, 1999.

9 Wells WM 3rd, Grimson WEL, Kikinis R, Jolesz FA: Statistical intensity correction and segmentation of MRI data. In: SPIE, Visualization in Biomedical Computing. ?????????? (eds). ??????????: ?????????, 1994; **2359**:13–24.

10 Wells WM 3rd, Grimson WEL, Kikinis R, Jolesz FA: Adaptive segmentation of MRI data. *IEEE Transactions on Medical Imaging* 1996; **15**(4):429–42.

11 Kikinis R, Guttmann CR, Metcalf D, Wells WM 3rd, Ettinger GJ, Weiner HL, Jolesz FA: Quantitative follow-up of patients with multiple sclerosis using MRI: technical aspects. *J Magn Reson Imaging* 1999; **9**:519–30.

12 Bajcsy R, Lieberson R, Reivich M: A computerized system for the elastic matching of deformed radiographic images to idealized atlas images. *J Comput Assist Tomogr* 1983; **7**:618–25.

13 Warfield SK, Zou KH, Wells WM 3rd: Validation of image segmentation and expert quality with an Expectation-Maximization algorithm. In: MICCAI: Fifth International Conference on Medical Image Computing and Computer-Assisted Intervention. Springer-Verlag, 2002; 298–306.

14 Warfield SK, Zou KH, Wells WM: Simultaneous truth and performance level estimation (STAPLE): an algorithm for the validation of image segmentation. *IEEE Trans Med Imaging* 2004; **23**:903–21.

15 Mazziotta JC, Toga AW, Evans A, Fox P, Lancaster J: A probabilistic atlas of the human brain: theory and rationale for its development. The International Consortium for Brain Mapping (ICBM). *Neuroimage* 1995; **2**:89–101.

16 Mazziotta JC, Toga AW, Evans AC, Fox PT, Lancaster JL: Digital brain atlases. *Trends Neurosci* 1995; **18**:210–1.

17 Brodmann K: Beitrage sur histologischen lokalisation der grosshirnrinde. Dritte mitteilung: Die rindenfelder der niederen affen. *Journal fur Psychologie und Neurologie (Leipzig)* 1905; **4**:177–226.

18 Matsui T, Kawamoto K, Iwata M, Kurent JE, Imai T, Ohsugi T, Hirano A: Anatomical and pathological study of the brain by CT scanner–1: anatomical study of normal brain. *Comput Tomogr* 1977; **1**: 3–43.

19 Schaltenband G, Wahren W, Walker EA: Atlas for Stereotaxy of the Human Brain. New York: Thieme Medical Publishers, Inc., 1977.

20 Talairach J, Tournoux P: Co-planar Stereotaxic Atlas of the Human Brain. New York: Thieme Medical Publishers, Inc., 1988.

21 Black KJ, Koller JM, Snyder AZ, Perlmutter JS: Template images for nonhuman primate neuroimaging: 2. Macaque. *Neuroimage* 2001; **14**:744–8.

22 Evans AC, Collins DL, Neelin P, MacDonald D, Kamber M, Marrett TS: Three dimensional correlative imaging: Applications in human brain mapping. In: Functional Neuroimaging and Technical Foundations. Thatcher, Hallett, John & Huerta (eds). San Diego: Academic Press, 1994; 145–61.

23 Friston KJ, Ashburner J, Frith CD, Pline JB, Heather JD, Frackowiak RSF: Spatial registration and normalization of images. *Human Brain Mapping* 1995; **2**:165–89.

24 Mazziotta J, Toga A, Evans A, Fox P, Lancaster J, Zilles K, Woods R, Paus T, Simpson G, Pike B, Holmes

C, Collins L, Thompson P, MacDonald D, Iacoboni M, Schormann T, Amunts K, Palomero-Gallagher N, Geyer S, Parsons L, Narr K, Kabani N, Le Goualher G, Boomsma D, Cannon T, Kawashima R, Mazoyer B: A probabilistic atlas and reference system for the human brain: International Consortium for Brain Mapping (ICBM). *Philos Trans R Soc Lond B Biol Sci* 2001; **356**:1293–322.

25 Mazziotta J, Toga A, Evans A, Fox P, Lancaster J, Zilles K, Woods R, Paus T, Simpson G, Pike B, Holmes C, Collins L, Thompson P, MacDonald D, Iacoboni M, Schormann T, Amunts K, Palomero-Gallagher N, Geyer S, Parsons L, Narr K, Kabani N, Le Goualher G, Feidler J, Smith K, Boomsma D, Hulshoff Pol H, Cannon T, Kawashima R, Mazoyer B: A four-dimensional probabilistic atlas of the human brain. *J Am Med Inform Assoc* 2001; **8**: 401–30.

26 Steinmetz H, Furst G, Freund HJ: Cerebral cortical localization: application and validation of the proportional grid system in MR imaging. *J Comput Assist Tomogr* 1989; **13**:10–19.

27 Desikan RS, Segonne F, Fischl B, Quinn BT, Dickerson BC, Blacker D, Buckner RL, Dale AM, Maguire RP, Hyman BT, Albert MS, Killiany RJ: An automated labeling system for subdividing the human cerebral cortex on MRI scans into gyral based regions of interest. *Neuroimage* 2006; **31**:968–80.

28 Herndon JG, Tigges J, Klumpp SA, Anderson DC: Brain weight does not decrease with age in adult rhesus monkeys. *Neurobiol Aging* 1998; **19**:267–72.

29 Mugler JP 3rd, Bao S, Mulkern RV, Guttmann CR, Robertson RL, Jolesz FA, Brookeman JR: Optimized single-slab three-dimensional spin-echo MR imaging of the brain. *Radiology* 2000; **216**:891–9.